Monthly Notices
of the
ROYAL ASTRONOMICAL SOCIETY

MNRAS **500,** 5515–5523 (2021)
Advance Access publication 2020 November 21

doi:10.1093/mnras/staa3611

# Instabilities and pulsations in models of the B-type supergiant $\kappa$ Cassiopeiae (HD 2905)

Abhay Pratap Yadav [1,2]★ Santosh Joshi[3] and Wolfgang Glatzel[4]★

[1]*Department of Physics & Astronomy, National Institute of Technology, Rourkela 769008, Odisha, India*
[2]*Government Model College Shahpura, Dindori 481990, Madhya Pradesh, India*
[3]*Aryabhatta Research Institute of Observational Sciences, Manora Peak, Nainital 263002, India*
[4]*Institut für Astrophysik (IAG), Georg-August-Universität Göttingen, Friedrich-Hund-Platz 1, D-37077 Göttingen, Germany*

Accepted 2020 November 13. Received 2020 November 11; in original form 2019 October 27

## ABSTRACT

For the B-type supergiant $\kappa$ Cassiopeiae (HD 2905), variabilities with periods between several hours and a few days have been observed both photometrically and spectroscopically. A recent study of this star by Simón-Díaz et al. has revealed variability with a dominant period of 2.7 d. To understand this variability, we present a linear non-adiabatic stability analysis with respect to radial perturbations for models of $\kappa$ Cassiopeiae. Instabilities associated with the fundamental mode and the first overtone are identified for models with masses between 27 and 44 $M_\odot$. For selected models, the instabilities are followed into the nonlinear regime by numerical simulations. As a result, finite amplitude pulsations with periods between 3 and 1.8 d are found. The model with a mass of 34.5 $M_\odot$ exhibits a pulsation period of 2.7 d consistent with the observations. In the nonlinear regime, the instabilities may cause a substantial inflation of the envelope.

**Key words:** instabilities – stars: massive – stars: mass-loss – stars: oscillations – supergiants – stars: winds, outflows.

## 1 INTRODUCTION

In several B-type stars, photometric as well as spectroscopic variabilities have been observed (see e.g. Waelkens et al. 1998; Saio et al. 2006; Aerts et al. 2010; Balona et al. 2011; Saesen et al. 2013; Rivinius, Baade & Carciofi 2016). Particularly, high-quality observations taken from space-based telescopes (e.g. *MOST*, *COROT*, *Kepler*, *BRITE*) have considerably enhanced our understanding of variabilities in B-type stars. Variability together with episodes of enhanced mass-loss have also been observed in some B-type supergiants (see e.g. Kraus et al. 2015; Haucke et al. 2018).

$\kappa$ Cassiopeiae or HD 2905 is a B-type supergiant situated in the constellation Cassiopeia. The presence of an astrosphere around $\kappa$ Cassiopeiae was revealed by observations taken with the *Infrared Astronomical Satellite* (van Buren & McCray 1988). Further high-resolution infrared observations taken with the *Spitzer Space Telescope* reveal that the astrosphere of $\kappa$ Cassiopeiae seems to have arcuate structure with several cirrus-type filaments (see Gvaramadze et al. 2011; Katushkina et al. 2018). From the existence and structure of the astrosphere around $\kappa$ Cassiopeiae, Katushkina et al. (2018) conclude and suggest that this star might be a runaway star.

Similar to other B-type supergiants, $\kappa$ Cassiopeiae exhibits variabilities and mass-loss. Using photometry with a 36 cm Cassegrain telescope, Elst (1979) has reported a variability with a period of 2.19 h for this star. However, Percy (1981) could not confirm this 2 h variability. Rather, he identified a variability with a period of the order of 7 d. Contrary to the findings of Percy (1981), observations taken at the UP State Observatory (now known as ARIES, Nainital) as reported by Badalia & Gurm (1982) indicate rapid variabilities with two periods of 1.7 and 1.4 h, respectively. Using photometry data of the *Hipparcos* catalogue, Koen & Eyer (2002) have found 2675 new variable stars including the supergiant $\kappa$ Cassiopeiae. These authors claim a photometric variability with a period of 2.6 d in this star. The supergiant $\kappa$ Cassiopeiae is also observed by the *BRITE* satellites. However, so far pulsations have not yet been found in the preliminary analysis of the collected data (Rybicka, Zocłońska & Tomić 2018). Based on 1141 high-resolution stellar spectra taken in a time span of approximately 2900 d, Simón-Díaz et al. (2018) have recently reported the presence of variabilities with periods mainly in the range between 2.5 and 10 d for $\kappa$ Cassiopeiae. A dominant period of 2.7 d present both in the spectral lines and in the *Hipparcos* space photometry has been identified by these authors. Although Simón-Díaz et al. (2018) have suggested that the variabilities might be associated with gravity modes or motions caused by subsurface convection, the cause of these variabilities is not properly understood.

Thus, with the motivation to understand the dominant variability of 2.7 d in $\kappa$ Cassiopeiae, we shall present here a linear non-adiabatic stability analysis of models for $\kappa$ Cassiopeiae. The result of instabilities will then be determined by following them into the nonlinear regime for selected unstable models using a fully conservative numerical scheme. This paper falls into five sections where a description of the models used is given in Section 2, and the linear stability analysis together with its results are discussed in Section 3. The nonlinear simulations and their results are presented in Section 4. A discussion and conclusions follow in Section 5.

★ E-mail: abhaypratapbhu@yahoo.com (APY); wglatze@astro.physik.uni-goettingen.de (WG)

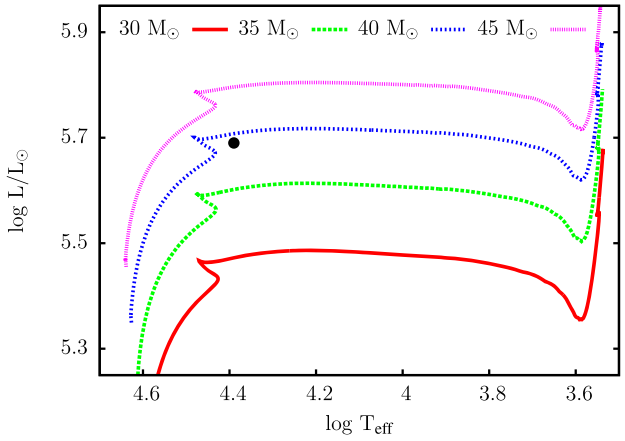


**Figure 1.** Evolutionary tracks of stars with solar chemical composition and having masses in the range between 30 and 45 $M_\odot$. The observed location of $\kappa$ Cassiopeiae in the Hertzsprung–Russell diagram is marked by a thick dot.

## 2 MODELS FOR $\kappa$ CASSIOPEIAE

Although the star $\kappa$ Cassiopeiae has been the subject of several studies (see e.g. Underhill 1979; Percy 1981; Hayes 1984; Katushkina et al. 2018), its fundamental parameters (in particular its mass) are not precisely known. For the present investigation, we adopt the effective temperature ($T_{\rm eff}$ = 24 600 K) and luminosity (log $L/L_\odot$ = 5.69) estimated by Simón-Díaz et al. (2018) using high-resolution spectra of $\kappa$ Cassiopeiae. These values are close to those determined by Kudritzki et al. (1999), Smartt et al. (2002), and Evans et al. (2004). Due to the uncertainty of the mass, we consider a range of models with masses between 27 and 44 $M_\odot$. This mass range covers the mass of 33 $M_\odot$ suggested for $\kappa$ Cassiopeiae by Searle et al. (2008) on the basis of stellar evolution calculations. Evolutionary tracks for models having solar chemical composition and masses of 30, 35, 40, and 45 $M_\odot$ respectively are shown in Fig. 1 where a thick dot corresponds to the observed position of $\kappa$ Cassiopeiae in the Hertzsprung–Russell (HR) diagram. These tracks have been generated by the 'mad star' stellar evolution code.[1] The position of $\kappa$ Cassiopeiae in the HR diagram suggests that models representing this star have masses below and close to 40 $M_\odot$ (see Fig. 1).

The amplitudes of radial eigenmodes decay exponentially from the stellar surface to the core. Thus, the latter may be disregarded when studying stellar stability (see e.g. Glatzel & Kiriakidis 1993; Glatzel, Kiriakidis & Fricke 1993; Saio 2011; Yadav & Glatzel 2016, 2017a). Accordingly, our present study is restricted to envelope models of $\kappa$ Cassiopeiae thus disregarding any influence of nuclear energy generation and nucleosynthesis. The envelope models with solar chemical composition ($X = 0.70$, $Y = 0.28$, and $Z = 0.02$; where $X$, $Y$, and $Z$ represent the mass fraction of hydrogen, helium, and heavy elements, respectively) are constructed by integrating the stellar structure equations as an initial value problem from the photosphere up to a sufficiently deep inner boundary (typically corresponding to a temperature of the order of $10^7$ K). For the photosphere, Stefan–Boltzmann's law and a standard prescription for the photospheric pressure (see e.g. section 11.2 of Kippenhahn, Weigert & Weiss 2012) are used as initial boundary conditions. Rotation as well as magnetic fields are disregarded and OPAL opacity tables (Rogers & Iglesias 1992; Iglesias & Rogers 1996; Rogers, Swenson & Iglesias 1996) are used for the opacity. For the onset of convection, Schwarzschild's criterion is used and the convection is treated according to standard mixing length theory (Böhm-Vitense 1958) with 1.5 pressure scale heights for the mixing length.

[1] www.astro.wisc.edu/~townsend/static.php?ref = ez-web

## 3 STABILITY ANALYSIS

To perform a linear stability analysis with respect to radial perturbations for models of $\kappa$ Cassiopeiae with parameters as discussed in Section 2, we have used the linearized perturbation equations given by Gautschy & Glatzel (1990b). This set of pulsation equations with four boundary conditions form a fourth-order eigenvalue problem which is solved using the Riccati method in a similar way as described by Gautschy & Glatzel (1990a). The solution of this system of equations leads to an infinite set of modes with complex eigenfrequencies ($\sigma_{\rm r} + {\rm i}\sigma_{\rm i}$). For convenience, they will be normalized with the global free fall time ($\sqrt{R^3/3GM}$; where $R$ is the stellar radius, $G$ denotes the gravitational constant, and $M$ stands for the stellar mass) of the corresponding model. The real part of the eigenfrequency corresponds to the pulsation frequency, whereas the imaginary part provides information about damping or excitation of the mode. In the normalization adopted, negative imaginary parts ($\sigma_{\rm i} < 0$) indicate excitation and instability while positive imaginary parts ($\sigma_{\rm i} > 0$) represent damping and stability. Interaction between pulsation and convection is still poorly understood. For simplicity, we have therefore used the 'frozen in approximation' as introduced by Baker & Kippenhahn (1965) in the present analysis. In this approximation, the Lagrangian perturbation of the convective flux is assumed to vanish. In previous studies (Glatzel & Mehren 1996; Yadav & Glatzel 2017b), it was found to hold as long as energy transport is dominated by radiation diffusion.

The results of the linear stability analysis are presented in terms of eigenfrequencies as a function of stellar mass in Fig. 2, where the real parts – corresponding to the pulsation frequency – are shown in Fig. 2(a) and the imaginary parts – indicating excitation or damping – are given in the Fig. 2(b). Negative imaginary parts ($\sigma_{\rm i} < 0$) correspond to excitation and instability. Real parts of the eigenfrequencies of excited modes are indicated by thick blue lines in Fig. 2(a). From Fig. 2, we deduce that all models considered with masses between 27 and 44 $M_\odot$ are unstable, where the instability affects the two lowest order modes (fundamental mode and first overtone). Similar to previous studies (e.g. Yadav & Glatzel 2017b), the growth rate and strength of the instabilities increase with the luminosity to mass ratio (see Fig. 2b). For higher order modes, mode coupling phenomena (for more details see, Gautschy & Glatzel 1990b), in particular avoided crossings can be identified in the modal diagram given in Fig. 2.

Although in many cases the results of the linear stability analysis are not substantially affected by the choice of the outer boundary conditions, their influence for the models considered here needs to be discussed. The outer boundary conditions for the perturbation equations are ambiguous because the outer boundary of the stellar model does not coincide with the physical outer boundary of the star. In fact for some stellar models, the choice of the outer boundary conditions was found to influence the presence of instabilities originating from regions close to the stellar surface (see e.g. Yadav & Glatzel 2016; Yadav, Kühnrich Biavatti & Glatzel 2018). In order to check the dependence on the outer boundary conditions of the results of the linear stability analysis for the models considered here, we have therefore performed the linear stability analysis of our models with different outer boundary conditions requiring zero heat storage and the gradient of compression to vanish there (for a detailed

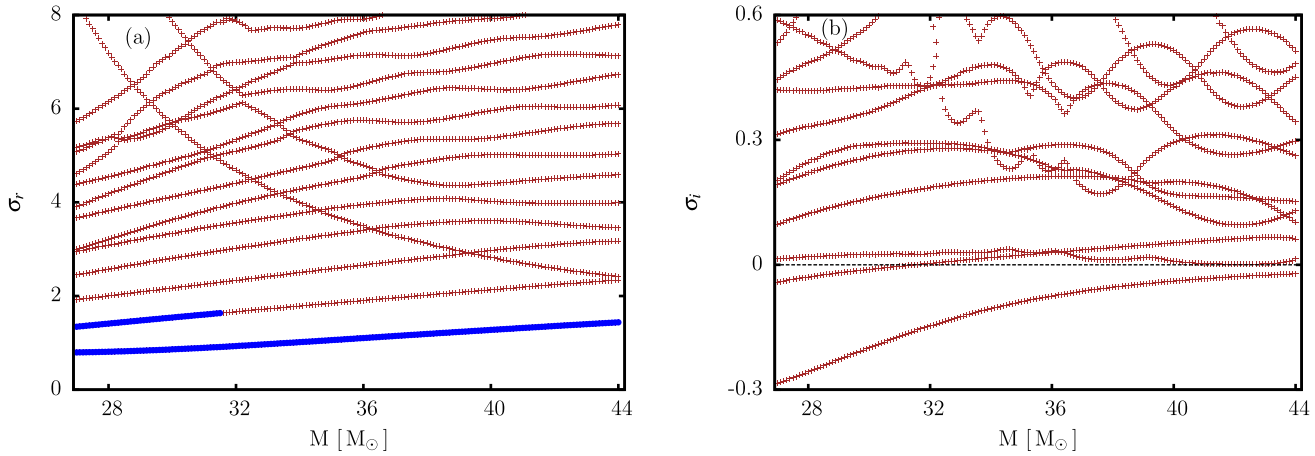


**Figure 2.** Real (a) and imaginary (b) parts of the eigenfrequencies as a function of mass for models of $\kappa$ Cassiopeiae having solar chemical composition, an effective temperature of $T_{\rm eff} = 24\,600$ K and a luminosity of $\log L/L_\odot = 5.69$. The eigenfrequencies are normalized with the global free fall time-scale. Thick blue lines in (a) and negative imaginary parts in (b) correspond to unstable modes. For the outer boundary conditions, vanishing of the Lagrangian pressure perturbation and the validity of Stefan–Boltzmann's law have been adopted.

discussion of these boundary conditions see Grott, Chernigovski & Glatzel 2005). These outer boundary conditions are used also for the subsequent numerical simulations following the instabilities into the nonlinear regime. The results of the linear stability analysis with these alternative boundary conditions are given in Fig. 3. Comparing Fig. 3 with Fig. 2, we note that for the stellar models considered the choice of the outer boundary conditions is of minor importance. The unstable modes found in Fig. 2 are also present in Fig. 3. Both the growth rates and the range of instabilities are almost identical for the different boundary conditions. However, an additional unstable mode is present in Fig. 3 for models with masses below 28 M$_\odot$.

The pulsation periods of various modes are given as a function of mass in Fig. 4. Similar to Figs 2 and 3, blue thick lines represent unstable modes. A red horizontal line corresponds to the period of 2.7 d observed in $\kappa$-Cassiopeiae. The pulsation period of the unstable fundamental mode lies between 3.9 and 1.6 d for the models considered while the period of the unstable first overtone lies below 2.3 d. From Fig. 4, we thus deduce that models with masses between 34 and 34.5 M$_\odot$ provide (linear) pulsation periods close to the observed period of 2.7 d.

## 4 INSTABILITIES IN THE NONLINEAR REGIME

The presence of at least two unstable modes in models of $\kappa$ Cassiopeiae has been found on the basis of a linear stability analysis. In order to determine the final fate of unstable models, the instabilities have to be followed into the nonlinear regime. As discussed by Yadav & Glatzel (2017b) instabilities of stellar models may lead to finite amplitude pulsations, eruptions of surface layers or the rearrangement of the stellar structure. To follow the instabilities into the nonlinear regime for selected unstable models of $\kappa$ Cassiopeiae, we have used the numerical scheme described by Grott et al. (2005). This numerical scheme provides the extremely high precision necessary for the simulation of finite amplitude pulsations and instabilities in the nonlinear regime. In particular, the energy balance is satisfied with extremely high precision. For the importance of a correct energy balance in the context of stellar pulsations we refer the reader to earlier studies (see e.g. Grott et al. 2005; Glatzel & Chernigovski 2016; Yadav & Glatzel 2017b). Accordingly, we have examined here the evolution of the error in the energy balance during the simulation of the evolution of an instability from hydrostatic equilibrium through the linear phase of exponential growth into the nonlinear regime. In the nonlinear regime, shock waves are expected to form. To handle the discontinuities caused by shocks, an artificial viscosity is introduced. It vanishes except close to a discontinuity. For details, the reader is referred to Grott et al. (2005) and Yadav & Glatzel (2017b).

### 4.1 Validation of the numerical scheme

Apart from satisfying the energy balance with high precision, we require the numerical scheme used for following instabilities into the nonlinear regime to represent the results of the independent linear stability analysis. For validation, we require the numerical code to start from a model in hydrostatic equilibrium and to pick up the physical instability with the period and growth rate as pre-determined independently by the linear analysis from numerical noise without any external perturbation. To prove this property of the scheme, we present the evolution of an instability from hydrostatic equilibrium through the linear phase of exponential growth into the nonlinear regime for a model with a mass of 34 M$_\odot$ in Fig 5. The linear stability analysis for this model of $\kappa$ Cassiopeiae provides an unstable mode where the real part of the associated eigenfrequency $\sigma_{\rm r} = 1.01$ corresponds to a pulsation period of 2.72 d. The imaginary part of the eigenfrequency $\sigma_{\rm i} = -0.11$ represents the growth rate of the mode. This period and growth rate should appear in the linear phase of the numerical simulation. As a result of the simulation the absolute velocity of the outermost grid point is given as a function of time in Fig. 5. The evolution of the instability starts from hydrostatical equilibrium with a numerical noise of the order of $10^{-4}$ cm s$^{-1}$. Without any external perturbation the code picks up an oscillatory exponentially growing instability: This is the expected linear phase of exponential growth. Both the growth rate and the pulsation period of 2.8 d observed in the simulation are consistent with the eigenfrequency provided and pre-determined by the linear stability analysis. After the linear phase the velocity amplitude saturates and the evolution finally enters the nonlinear phase of finite amplitude pulsations. Thus, the numerical code has been shown to pick up

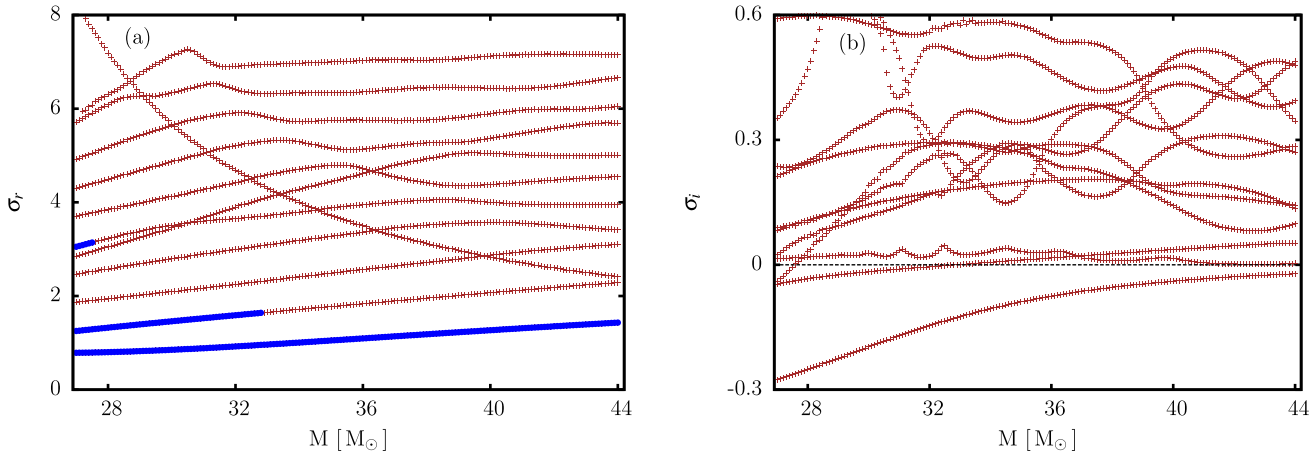


**Figure 3.** Same as Fig. 2 but for boundary conditions consistent with those used in the subsequent nonlinear simulations.

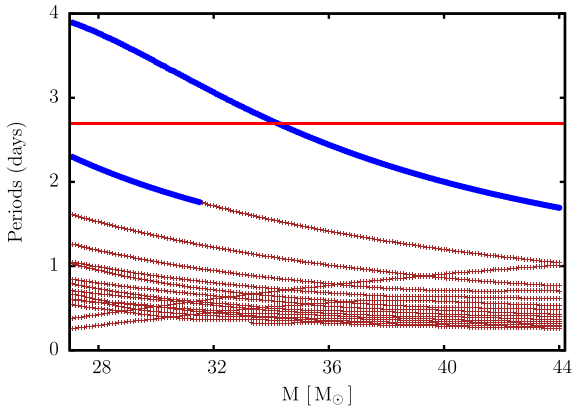


**Figure 4.** Periods of various modes in models of $\kappa$ Cassiopeiae. Thick blue lines correspond to unstable modes and the red line denotes the observed dominant period of 2.7 d. Models in the mass range between 34 and 34.5 M$_\odot$ exhibit an unstable fundamental mode with a period close to the observed value.

the correct physical instability without any external manipulation. Additional numerical instabilities do not seem to be present.

### 4.2 Results of the nonlinear simulations

All models for $\kappa$ Cassiopeiae with masses in the range between 27 and 44 M$_\odot$ are unstable according to the linear stability analysis. In order to determine the final fate of the unstable models, we have followed the instabilities into the nonlinear regime for selected cases. The results of the nonlinear simulation for a model with a mass of 27 M$_\odot$ are shown in Fig. 6: radius (a), temperature (b), and absolute velocity (c) at the outermost grid point are given as a function of time. The evolution of the velocity (starting from hydrostatic equilibrium) shows that the code picks up the instability from numerical noise with an amplitude of the order of $10^{-4}$ cm s$^{-1}$, the subsequent linear phase is characterized by oscillatory exponential growth. A saturation of the velocity amplitude is found, when the nonlinear regime is reached. In this phase the envelope is inflated (see Fig. 6a) and the radius of the outermost grid point increases approximately by a factor of nine compared to its initial hydrostatic value. As a consequence, the temperature at the outermost grid point drops to $\approx$ 5000 K and the simulation had to be stopped, since opacity data were

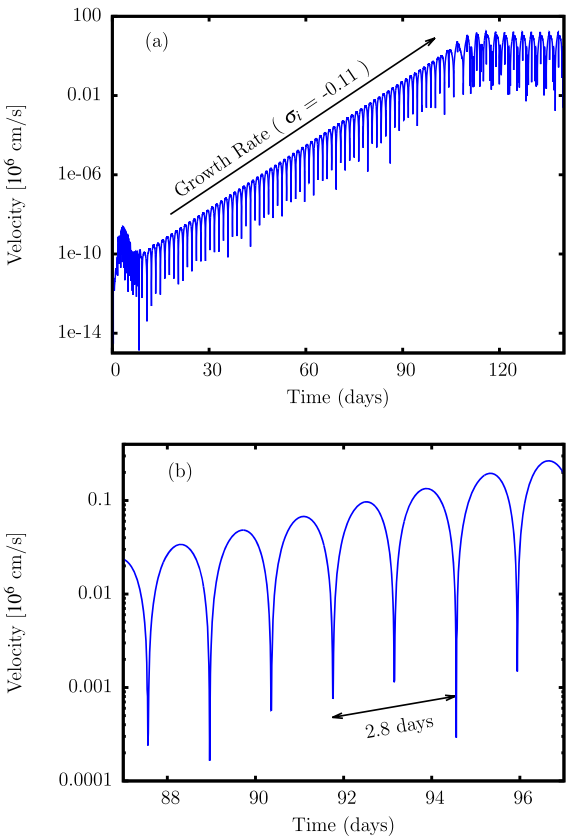


**Figure 5.** Validation of the numerical scheme: For a numerical simulation the absolute velocity of the outermost grid point is shown as a function time. The simulation starts from hydrostatic equilibrium, undergoes the linear phase of exponential growth, and finally ends in nonlinear saturation. For the model considered, the linear stability analysis provides an unstable mode with a real part of the eigenfrequency of $\sigma_r = 1.01$ corresponding to a pulsation period of 2.72 d and an imaginary part of the eigenfrequency of $\sigma_i = -0.11$. In the linear phase, the growth rate observed in the numerical simulation in (a) is consistent with the value for $\sigma_i$ as determined by the linear theory (slope of the arrow). Moreover, the pulsation period of 2.8 d deduced from (b) in the linear phase of the simulation is close to the value of 2.72 d obtained from the linear analysis.

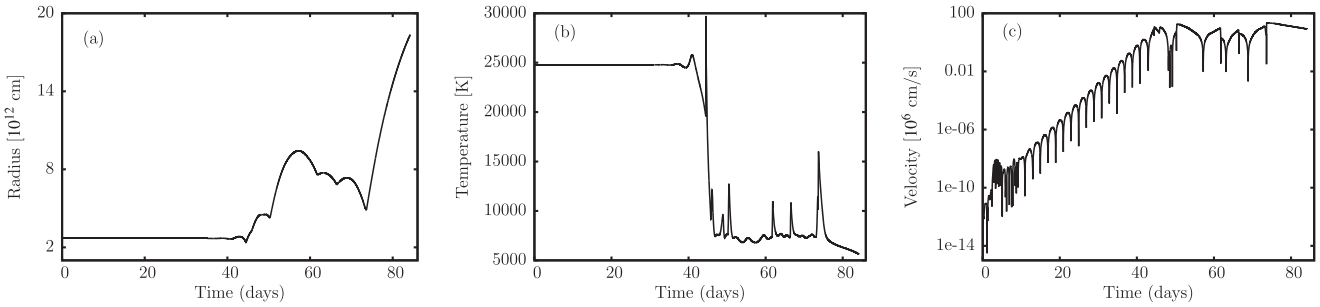


**Figure 6.** Evolution of an instability into the nonlinear regime for a model of $\kappa$-Cassiopeiae (HD 2905) having a mass of 27 $M_\odot$: radius (a), temperature (b), and absolute velocity (c) of the outermost grid point are given as a function of time. Note that in this case the instability leads to a substantial inflation of the model. As a consequence, the pulsation period is increased compared to the linearly determined value.

no longer available. The maximum velocity reached in the nonlinear regime amounts to 224 km $s^{-1}$ and corresponds to 43 per cent of the escape velocity of the model (517 km $s^{-1}$). We note that some simulations of instabilities in models for massive B-type stars have provided evidence for the instability driven maximum velocity to exceed the escape velocity of the corresponding models (see Glatzel et al. 1999; Yadav & Glatzel 2016) which implies direct mass-loss due to instabilities. With the reservation that the simulation is not yet complete, we find for the model of $\kappa$ Cassiopeiae considered the maximum velocity to remain well below the escape velocity. However, the substantial inflation of the envelope in the nonlinear regime may be taken as another indication for mass-loss.

The evolution of instabilities into the nonlinear regime for a model with a mass of 32 $M_\odot$ is illustrated in Fig. 7: radius (a), absolute velocity (b), and temperature (c) at the outermost grid point together with the variation of the bolometric magnitude (d) are presented as a function of time. The velocity of the outermost grid point starts from numerical noise in hydrostatic equilibrium and finally saturates after the linear phase of exponential growth in the nonlinear regime 80 d after start with a maximum velocity close to 126 km $s^{-1}$. Thus finite amplitude pulsations are the result of the instability in this model, which may also be deduced from the evolution of the radius (Fig. 7a). The final mean value of the radius is approximately 30 per cent larger than the initial hydrostatic value and the inflation of the radius is associated with a decrease of the temperature (Fig. 7c). We emphasize that the temperature at the outermost grid point referred to here is not necessarily related to the effective temperature of the model, since the relative position of the photosphere may differ from its initial hydrostatic location, in particular, when inflation is significant. Moreover, it may vary during the pulsation cycle. The variation of the bolometric magnitude (d) exhibits a well-defined period of 3 d.

Similar to the model with a mass of 32 $M_\odot$, we have followed the instability into the nonlinear regime for the model with a mass of 34.5 $M_\odot$. The results for this model presented in Fig. 8 are similar to those obtained for 32 $M_\odot$. The velocity saturates with a maximum value of 110 km $s^{-1}$ in the nonlinear regime and the inflation of the radius (Fig. 8a) is less pronounced than for 32 $M_\odot$. A period of 2.7 d for the final finite amplitude pulsations is obtained from the variation of the bolometric magnitude (c). It agrees with the observed dominant period of $\kappa$-Cassiopeiae (HD 2905) reported by Simón-Díaz et al. (2018).

Quantities associated with outermost grid point are generally used to study envelope inflation, pulsation period and energy budget during simulation in nonlinear regime. However, quantities linked with outermost grid point may not represent the photospheric values. Therefore for model with mass 34.5 $M_\odot$, radius (a), absolute velocity (b), temperature (c), and density (d) associated with grid points near the photosphere are given in Fig. 9. To identify the location of photospheric grid point in our simulations, we have used Stefan–Boltzmann relation. The outermost grid point where total flux is equal to $\sigma T^4$ (here $\sigma$ and T are Boltzmann constant and temperature, respectively) has been taken as an approximate location of the photosphere. As found in Fig. 8, a period of 2.7 d is also present in the variation profile of the mentioned quantities in Fig. 9. Compared to the hydrostatic value of radius (see Fig. 8a), the model exhibits finite amplitude pulsation with slightly inflated mean radius ($\approx 2.87 \times 10^{12}$ cm). The maximum-to-minimum variation in bolometric magnitude is found to be approximately 0.2 mag which is larger than the value determined by Simón-Díaz et al. (2018) using HIPPARCOS data.

Apart from 2.7 d variability, Simón-Díaz et al. (2018) have found additional frequencies in the range of 0.1 and 0.4 $d^{-1}$. Comparison of the shape of the observed bolometric magnitude profile with theoretically determined bolometric magnitude profile has to be done with caution as the latter is resulting from a single instability corresponding to a linear period of 2.7 d while several frequencies are present in the observed profile. Maximum-to-minimum variation of absolute velocity associated with this grid point (Fig. 9b) is around 240 km $s^{-1}$ which is considerably larger than the values (30 km $s^{-1}$) determined by Simón-Díaz et al. (2018) using photospheric spectral lines such as Si III and Si IV. These authors have also reported that the amplitude of variability increases from deep photospheric lines to the lines formed in stellar winds. During the finite amplitude pulsation phase, temperature varies in the range of 26 820 and 17 500 K with variation mostly between 17 800 and 20 000 K (see Fig. 9c). From spectroscopic analysis, Simón-Díaz et al. (2018) find surface temperature in the range of 23 700–25100 K with average value of 24 600 ± 300 K. The value of artificial viscosity parameter can affect the temperature variation during the finite amplitude pulsation as shown by Yadav & Glatzel (2017b). Variation profile of density (Fig. 9d) exhibits sharp peaks with a separation 2.7 d.

Results of the numerical simulation for models with masses of 38, 40, and 42 $M_\odot$ are presented in Figs 10–12, respectively. In these figures, the radius (a) and the absolute velocity (b) at the outermost grid point together with the variation of the bolometric magnitude (c) are given as a function of time. The velocity starts from numerical noise at the level of $10^{-4}$ cm $s^{-1}$ and finally saturates in the nonlinear regime with maximum values of 95, 109, and 108 km $s^{-1}$ for the models with masses of 38, 40, and 42 $M_\odot$, respectively. Thus, the instabilities of models with masses of 38, 40, and 42 $M_\odot$ lead to finite amplitude pulsations with periods of 2.2, 2.0, and 1.8 d, respectively (see Figs 10c, 11c, and 12c). From Figs 10(a), 11(a), and 12(a), we still deduce a slight inflation of the radius in the nonlinear regime.

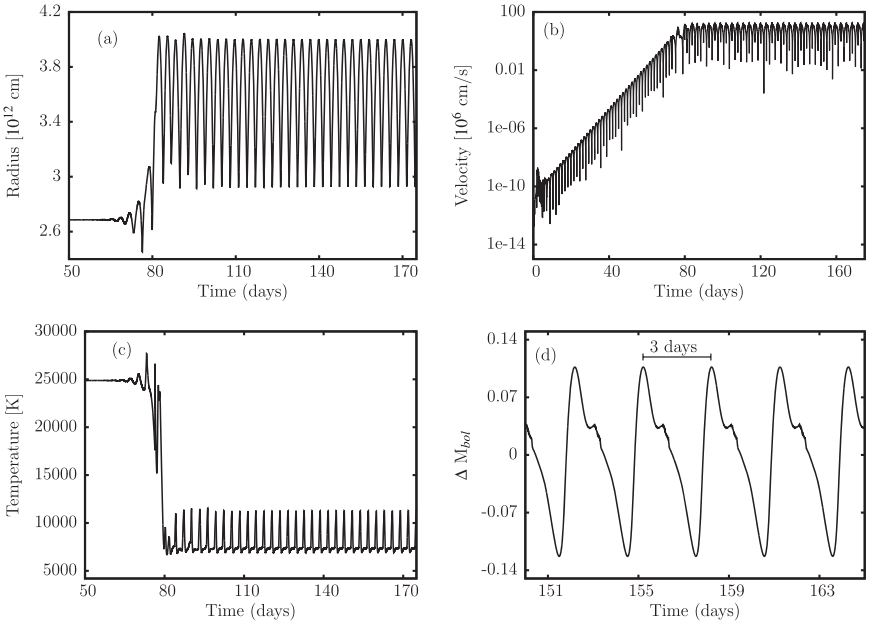


**Figure 7.** Evolution of an instability into the nonlinear regime for a model of $\kappa$-Cassiopeiae (HD 2905) with a mass of 32 $M_{\odot}$: radius (a), absolute velocity (b), and temperature (c) at the outermost grid point and variations of the bolometric magnitude (d) are given as a function of time. This model finally exhibits finite amplitude pulsations with a period of 3 d.

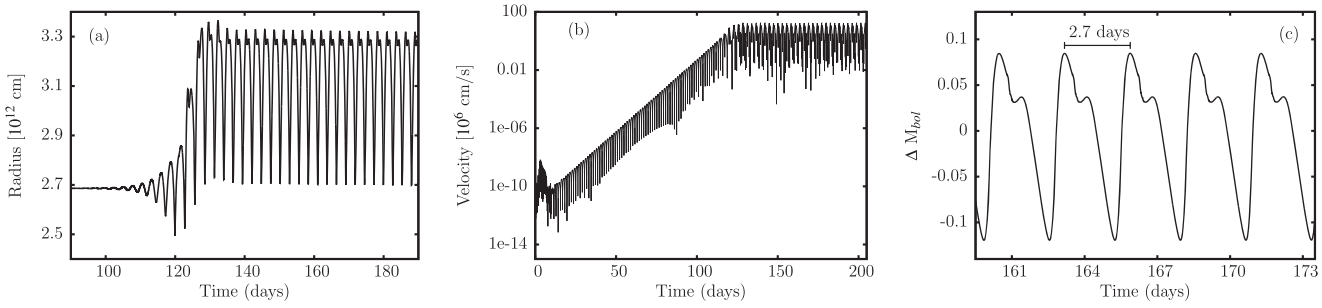


**Figure 8.** Same as Fig. 7 but for a model of $\kappa$-Cassiopeiae (HD 2905) with a mass of 34.5 $M_{\odot}$: radius (a), absolute velocity (b) at the outermost grid point and variations of the bolometric magnitude (c) are given as a function of time. This model finally exhibits finite amplitude pulsations with a period of 2.7 d, which exactly matches the observed dominant period of the star.

## 5 DISCUSSION AND CONCLUSION

In order to understand the variabilities observed in $\kappa$ Cassiopeiae (see e.g. Simón-Díaz et al. 2018), we have performed a linear non-adiabatic stability analysis for models of this supergiant. All models considered with masses in the range between 27 and 44 $M_{\odot}$ are unstable. The instabilities are associated with low-order modes (fundamental mode and first overtone) while higher order modes are damped (see Fig. 2). As expected, growth rate and strength of the instabilities increase with the luminosity to mass ratio. If the luminosity to mass ratio exceeds $10^4$ in solar units (which holds for all models considered here), dynamical instabilities are to be expected (see e.g. Glatzel 1994). In particular, strange modes and associated instabilities are typically found in stellar models with luminosity to mass ratios in excess of $10^4$ (solar units). In general, strange modes are related to mode coupling phenomena appearing as instability bands and avoided crossings. Prominent examples are models of massive zero-age main sequence stars (Yadav & Glatzel 2017a), Wolf Rayet stars (Kiriakidis, Glatzel & Fricke 1996), and HdC stars (Gautschy & Glatzel 1990b). In modal diagrams of models for $\kappa$ Cassiopeiae (see, e.g. Fig. 2), mode coupling phenomena can be identified for higher order modes. However, they are not associated with instability bands. On the other hand, mode coupling effects do not seem to be involved in the unstable low-order modes which appear to be ordinary low-order p-modes. However, to identify the physical origin of the instabilities found here as driven by resonances (mode coupling, strange modes) or by the $\kappa$-mechanism requires application of the non-adiabatic reversible approximation (Gautschy & Glatzel 1990b). We intend to present a corresponding analysis in a forthcoming paper. The stability analysis was repeated with different boundary conditions (see Fig. 3) to test their influence on the results. In fact, for models of $\kappa$ Cassiopeiae the choice of boundary conditions is largely irrelevant, at least as long as the instabilities and the range of unstable models are concerned. The pulsation frequency of the unstable fundamental mode lies between 3.9 and 1.6 d for masses of the stellar model between 27 and 44 $M_{\odot}$.

In order to determine the final fate of the unstable models, the instabilities have been followed into the nonlinear regime by numerical

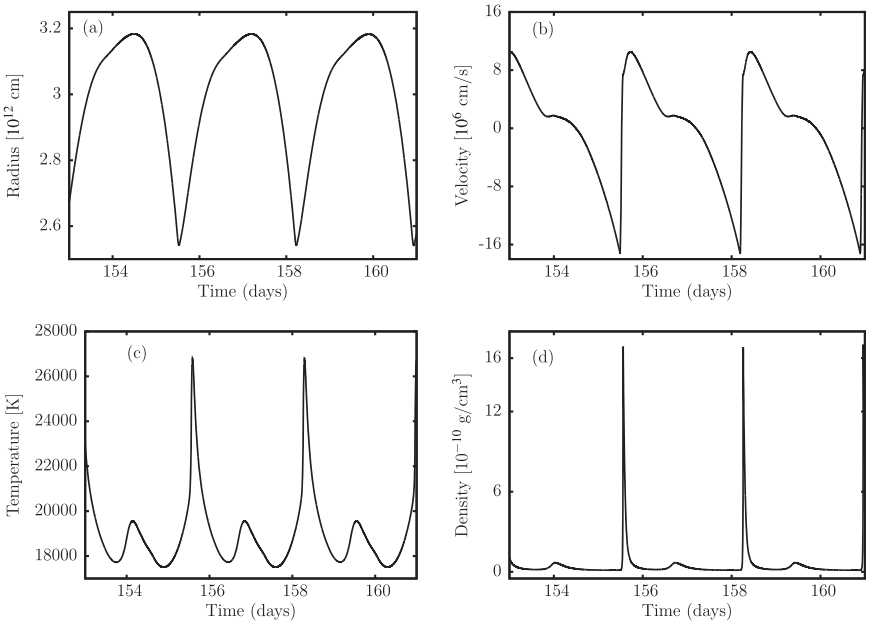


**Figure 9.** Finite amplitude pulsation with a period of 2.7 d in the model with a mass of 34.5 $M_\odot$. Variations in radius (a), absolute velocity (b), temperature (c), and density (d) are given to a grid point close to the photosphere.

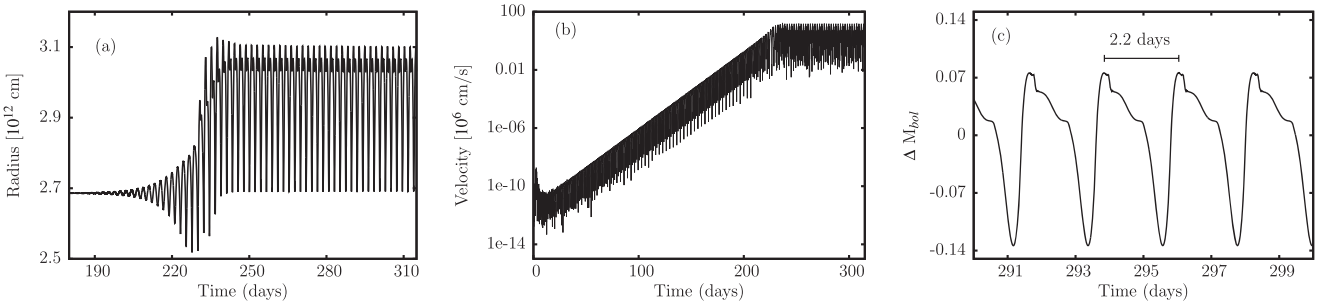


**Figure 10.** Evolution of an instability into the nonlinear regime for a model of $\kappa$-Cassiopeiae (HD 2905) with a mass of 38 $M_\odot$: radius (a) and absolute velocity (b) at the outermost grid point and variations of the bolometric magnitude (c) are given as a function of time. This model finally exhibits finite amplitude pulsations with a period of 2.2 d.

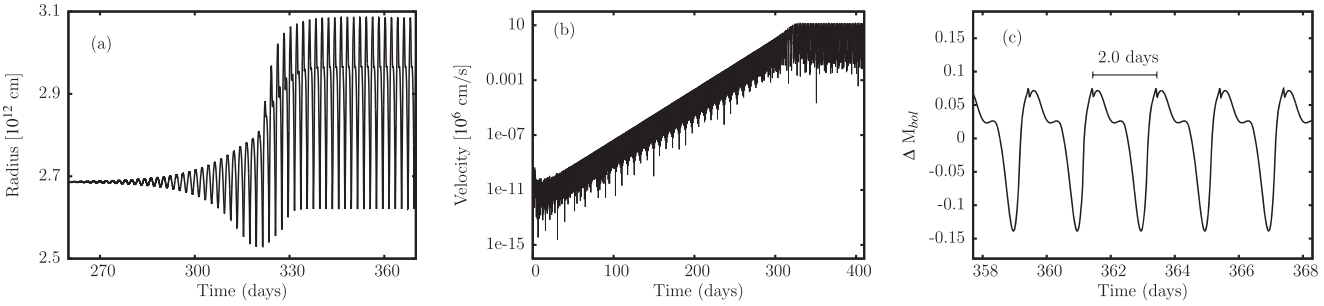


**Figure 11.** Same as Fig. 10 but for a model with a mass of 40 $M_\odot$. Here the instability leads to finite amplitude pulsations with a period of 2 d.

simulation for selected cases. Any simulation of stellar instabilities and finite amplitude stellar pulsations requires an extremely high accuracy which can be achieved only by a fully conservative numerical scheme. In particular, the energy balance needs to be correct to a very high degree of precision. We have adopted a numerical scheme which meets all these requirements (for details see e.g. Grott et al. 2005; Yadav et al. 2018). In order to ensure that the code picks up and follows the physical instabilities, it was validated by comparing periods and growth rates of the instabilities appearing in the simulation (in the linear phase of exponential growth) with the independently pre-determined values provided by the linear stability analysis (see Section 4.1). For models with masses below 29 $M_\odot$, the

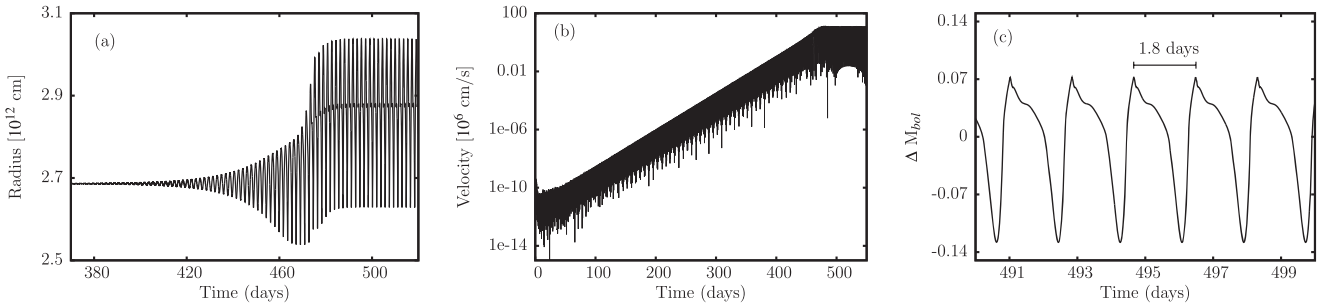


**Figure 12.** Same as Fig. 10 but for a model with a mass of 42 $M_\odot$. Here the instability leads to finite amplitude pulsations with a period of 1.8 d.

instabilities lead to a substantial inflation of the radius (see Fig. 6). For higher masses, finite amplitude pulsations with periods between 1 and 3 d are the final fate of the unstable models considered. Ground- and space-based observations of $\kappa$ Cassiopeiae, Simón-Díaz et al. (2018) have revealed a variability with a dominant period of 2.7 d for this object. On the other hand, finite amplitude pulsations with a period of 2.7 d are found as the final result when simulating the evolution of the instability into the nonlinear regime of the model for $\kappa$ Cassiopeiae with a mass of 34.5 $M_\odot$. Thus the observed variability with a period of 2.7 d may be explained by the instability of the fundamental radial mode of an object with a mass of 34.5 $M_\odot$. In addition to the 2.7 d period, the variability of $\kappa$ Cassiopeiae exhibits additional periods in the range between 2.5 and 10 d (Simón-Díaz et al. 2018). According to our linear stability analysis the model with the lowest mass (27 $M_\odot$) provides two unstable modes with periods of 2.3 and 3.9 d respectively. Thus both from the linear analysis and the nonlinear simulations we conclude that variabilities with periods above 3.9 d cannot be explained by radial unstable modes of $\kappa$ Cassiopeiae. Variabilities with periods above 3.9 d might be due to gravity modes. Their study requires a linear non-adiabatic stability analysis with respect to non-radial perturbations which will be the primary objective of an extension of the present study. Earlier studies of $\kappa$ Cassiopeiae report on variabilities on time-scales between 1 and 2 h (see e.g. Elst 1979; Badalia & Gurm 1982). However, variability with short periods (of the order of hours) has not been found by Simón-Díaz et al. (2018). Thus, the existence of long-lived short-period variabilities in $\kappa$ Cassiopeiae is yet to be confirmed. In this context, observations of TESS may contribute significantly to our understanding of the variabilities in $\kappa$ Cassiopeiae.

From this study which has been restricted to considering radial perturbations we infer that the dominant variability of $\kappa$ Cassiopeiae with a period of 2.7 d may be understood as a radial mode pulsation. However, we note that the theoretical light curve is differing from the observed light curve of Simón-Díaz et al. (2018). Shape and amplitude of the theoretical light curve depends on parameters including the number of unstable modes, strength of present instabilities and value of artificial viscosity parameter. This study is a first step to understand the variability of 2.7 d using linear stability analysis in combination with nonlinear simulations. To compare the light curve, we need to perform extensive nonlinear simulations. Additional observed variabilities of this star need further attention. In particular, variabilities with periods above 10 d being compatible with g-mode pulsations have been observed in $\kappa$ Cassiopeiae (Simón-Díaz et al. 2018). Moreover, in addition to radial instabilities, non-radial instabilities have been identified in models of B-type stars (e.g. Gautschy & Saio 1993; Glatzel & Mehren 1996; Saio et al. 2006; Saio 2011). Therefore, to complete and improve our understanding of variabilities in $\kappa$ Cassiopeiae, a linear non-adiabatic stability analysis with respect to non-radial perturbations is inevitable. These issues will be presented in a forthcoming paper.

## ACKNOWLEDGEMENTS

APY gratefully acknowledges the hospitality and support of the Aryabhatta Research Institute of Observational Sciences (ARIES), Nainital where a part of this study has been performed. We thank the anonymous referee for constructive comments to improve this paper.

## DATA AVAILABILITY

Data derived and used to perform the present study will be available on reasonable request to the corresponding author.

## REFERENCES

Aerts C. et al., 2010, A&A, 513, L11
Badalia J. K., Gurm H. S., 1982, Inf. Bull. Var. Stars, 2163
Baker N., Kippenhahn R., 1965, ApJ, 142, 868
Balona L. A. et al., 2011, MNRAS, 413, 2403
Böhm-Vitense E., 1958, ZAp, 46, 108
Elst E. W., 1979, Inf. Bull. Var. Stars, 1697
Evans C. J., Crowther P. A., Fullerton A. W., Hillier D. J., 2004, ApJ, 610, 1021
Gautschy A., Glatzel W., 1990a, MNRAS, 245, 154
Gautschy A., Glatzel W., 1990b, MNRAS, 245, 597
Gautschy A., Saio H., 1993, MNRAS, 262, 213
Glatzel W., 1994, MNRAS, 271, 66
Glatzel W., Chernigovski S., 2016, MNRAS, 457, 1190
Glatzel W., Kiriakidis M., 1993, MNRAS, 262, 85
Glatzel W., Mehren S., 1996, MNRAS, 282, 1470
Glatzel W., Kiriakidis M., Fricke K. J., 1993, MNRAS, 262, L7
Glatzel W., Kiriakidis M., Chernigovskij S., Fricke K. J., 1999, MNRAS, 303, 116
Grott M., Chernigovski S., Glatzel W., 2005, MNRAS, 360, 1532
Gvaramadze V. V., Kniazev A. Y., Kroupa P., Oh S., 2011, A&A, 535, A29
Haucke M., Cidale L. S., Venero R. O. J., Curé M., Kraus M., Kanaan S., Arcos C., 2018, A&A, 614, A91
Hayes D. P., 1984, AJ, 89, 1219
Iglesias C. A., Rogers F. J., 1996, ApJ, 464, 943
Katushkina O. A., Alexashov D. B., Gvaramadze V. V., Izmodenov V. V., 2018, MNRAS, 473, 1576
Kippenhahn R., , Weigert A., Weiss A., 2012, Stellar Structure and Evolution. Springer, Berlin
Kiriakidis M., Glatzel W., Fricke K. J., 1996, MNRAS, 281, 406
Koen C., Eyer L., 2002, MNRAS, 331, 45
Kraus M. et al., 2015, A&A, 581, A75
Kudritzki R. P., Puls J., Lennon D. J., Venn K. A., Reetz J., Najarro F., McCarthy J. K., Herrero A., 1999, A&A, 350, 970
Percy J. R., 1981, Inf. Bull. Var. Stars, 1946

Rivinius T., Baade D., Carciofi A. C., 2016, A&A, 593, A106
Rogers F. J., Iglesias C. A., 1992, ApJS, 79, 507
Rogers F. J., Swenson F. J., Iglesias C. A., 1996, ApJ, 456, 902
Rybicka M., Zocłońska E., Tomić S., 2018, in Wade G. A., Baade D., Guzik J. A., Smolec R., eds, Proc. Polish Astron. Soc. Vol. 8, 3rd BRITE Science Conference, Polish Astronomical Society, Poland. p. 134
Saesen S., Briquet M., Aerts C., Miglio A., Carrier F., 2013, AJ, 146, 102
Saio H., 2011, MNRAS, 412, 1814
Saio H. et al., 2006, ApJ, 650, 1111
Searle S. C., Prinja R. K., Massa D., Ryans R., 2008, A&A, 481, 777
Simón-Díaz S., Aerts C., Urbaneja M. A., Camacho I., Antoci V., Fredslund Andersen M., Grundahl F., Pallé P. L., 2018, A&A, 612, A40
Smartt S. J., Lennon D. J., Kudritzki R. P., Rosales F., Ryans R. S. I., Wright N., 2002, A&A, 391, 979
Underhill A. B., 1979, ApJ, 234, 528
van Buren D., McCray R., 1988, ApJ, 329, L93
Waelkens C., Aerts C., Kestens E., Grenon M., Eyer L., 1998, A&A, 330, 215
Yadav A. P., Glatzel W., 2016, MNRAS, 457, 4330
Yadav A. P., Glatzel W., 2017a, MNRAS, 465, 234
Yadav A. P., Glatzel W., 2017b, MNRAS, 471, 3245
Yadav A. P., Kühnrich Biavatti S. H., Glatzel W., 2018, MNRAS, 475, 4881

This paper has been typeset from a TEX/LATEX file prepared by the author.